ORIGINAL ARTICLE

Investigation of mechanical properties and elucidation of factors affecting wood-based structural panels under embedment stress with a circular dowel i: analysis of the influence of various conditions on the embedment properties

Ryutaro Sudo[1,2]*, Kenji Aoki[1] and Masahiro Inayama[1]

Abstract

Embedment properties are vital to timber structural designs, and many types of wood-based structural panels have been developed for diverse uses. Comprehensive and systematic studies regarding the embedment properties of wood-based structural panels are limited. In this study, a jig that allows the observation of fracture processes is developed, and a monotonic tensile embedment test is conducted on plywood, oriented strandboard (both strong and weak axes), particleboard, medium density fiberboard, and hardboard. The parameters used in the test are the dowel diameter, pilot hole size, and end and edge distances. The effects of these parameters on the embedment properties (i.e., the failure mode, ductility, maximum stress, and yield stress) are discussed comprehensively. The failure mode is determined by the edge distance. At a sufficient edge distance, ductile failure occurs, and the load is maintained until the remaining end distance reaches a certain value. The maximum stress and yield stress are analyzed quantitatively via standardized multiple regression analysis. The results suggest the following: (i) The ratio of the in-plane strength to the internal bond strength is related to the failure behavior; (ii) the dowel diameter, fiber direction, and load levels affect the stress spread pattern of the embedment pressure.

Keywords Wood-based structural panel, Plywood (PW), Oriented strand board (OSB), Particleboard (PB), Medium density fiberboard (MDF), Hardboard (HB), Bearing, Embedment, Pilot hole, Edge distance, End distance, Standardized multiple regression analysis (SMRA)

*Correspondence:
Ryutaro Sudo
sudo-ryutaro282@g.ecc.u-tokyo.ac.jp; sudoryutaro0513@ffpri.affrc.go.jp
[1] Department of Biomaterials Sciences, Graduate School of Agricultural and Life Sciences, The University of Tokyo, 1-1-1 Yayoi, Bunkyo-Ku, Tokyo, Japan
[2] Forestry and Forest Products Research Institute, 1 Matsunosato, Tsukuba, Ibaraki 305-8687, Japan

Introduction

Many types of wood-based panels have been developed recently, with each composed of different types of elements as raw materials [1]. These panels are often used for interior paneling. Additionally, they have been employed in structural applications.

The performance of a timber structure is generally determined by the joint performance. When the joints are deformed, hard cylindrical dowels (e.g., nails and bolts) become embedded in the wooden members—a

Sudo *et al. Journal of Wood Science*   (2023) 69:18

Page 2 of 15

phenomenon known as "embedment"—and their mechanical properties significantly affect structural designs. Therefore, the performance of joints, such as the yield load [2] and initial stiffness [3], can be predicted based on the embedment properties.

The embedment properties of timber and other types of wood-based materials used for columns and beams have been investigated extensively. Examples include comprehensive experimental studies using the diameter of the dowel as a main parameter [4, 5] and those pertaining to the relationship between the pilot hole and the embedment properties of timber [6]. To theoretically elucidate the fracture mechanisms and physical influencing factors of wood subjected to embedment pressure, researchers have estimated the splitting failure strength caused by embedment stress using fracture mechanics [7, 8] and verified the relationship between embedment properties and the friction coefficient of dowels and members [9–11]. To clarify the failure process by detailed observations, advanced methods such as digital image correlation and computed tomography scans have been applied [11–13]. Additionally, researchers have developed advanced analytical methods considering softened or damaged zones around dowels, which have been applied to estimate loads at large deformation ranges, including cases with decreasing loads [14, 15].

In Japan and other countries, the embedment resistance of wood-based structural panels is regarded as equally important as that of timber, and performance standards of some types of panels are defined in JIS [16, 17]. Standard test methods, called the lateral nail resistance test, have been defined by JIS [16, 17], JAS [18, 19], or ASTM [20]. In addition, the embedment properties have been investigated. For example, researchers have investigated the embedment strength of PB [21–24], a performance degradation model based on long-term exposure [24–26], the effect of the density profile of MDFs [27], and the effect of the fiber direction of PWs on the initial stiffness of embedment stress [28].

However, these studies cannot be classified as systematic and comprehensive owing to the limited parameters used. Furthermore, the embedment properties were measured as part of the performance of the panels rather than as a main objective of the studies. Wood-based structural panels are primarily used structurally in sheathed shear walls and floors. Therefore, determining the method of constructing joints for wood-based structural panels based on specification rules is sufficient for practical purposes, whereas knowledge regarding their fundamental performance is still inadequate.

Currently, wood-based structural panels are used in new applications owing to the increasing scale of timber structures and design diversification [29]. The development of new materials such as mass plywood panels [30] is expected to support this trend. In addition, many types of wood-based structural panels exist, with each composed of different-size raw wood elements. Therefore, promoting the structural use of wood-based structural panels encourages their cascade use [31], which is meaningful from an environmental perspective.

Limited research has been conducted on the embedment properties of wood-based panels, which will be further discussed in the following paragraphs. Experimental data regarding the embedment properties of timber include the yield load, maximum load, initial stiffness, and ductility. The influencing factors have been identified, and regression equations have been used to determine the characteristic values using these factors. Furthermore, researchers have investigated the effects of edge and end distances on the failure modes, elucidated each failure mechanism, and theoretically estimated the characteristic values corresponding to the failure modes.

In contrast, comprehensive and systematic studies regarding the embedment properties of wood-based panels are few, and owing to insufficient experimental data, factors affecting these properties have not been elucidated. The change in the failure mode by the end and edge distances, which are generally used as parameters to investigate the embedment properties of timber, has not been clarified. Similarly, the failure mechanism of wood-based panels under embedment forces has not been revealed. Furthermore, no single paper has provided a comprehensive analysis of multiple characteristic values. Most related studies have focused primarily on the maximum stress, whereas ductility has not been investigated. From the view of actual use, the criteria for the edge distance of a panel sheathed shear wall are customary, and an appropriate manual for the edge distance corresponding to the connection type or a wood-based panel does not exist.

To enhance the structural use of wood-based panels, clarification is required regarding the effect of the parameters, as used in a previous study pertaining to the embedment properties of timber, on the various characteristic values and, subsequently, the failure mode and mechanisms. This paper presents the basis for theoretical studies pertaining to the embedment properties of wood-based panels and contributes to the derivation of an estimation equation. In addition, the findings of this study contribute to the actual application, for example, the selection of wood-based panels for the desired structural form and the appropriate configuration of the connections.

In this study, embedment tests were performed on five types of wood-based structural panels to observe the fracture processes. In addition to the panel type, the

Table 1 Fundamental properties of the panels

		Density (kg/m³)	MC (%)	In-plane tensile properties		Internal bond properties		In-plane shear properties		Other information
				Strength (MPa)	Elastic modulus (GPa)	Strength (MPa)	Elastic modulus (GPa)	Strength (MPa)	Elastic modulus (GPa)	
PW	Ave	416	11.1	13.5	5.28	0.930	0.0151	4.72	0.619	Wood species: *Cryptomeria japonica* (Japanese cedar) number of layers: 5, class: 2nd, use: structural [18]
	S. D	20	1.2	4.0	1.56	0.245	0.0089	0.14	0.095	
OSB	Ave	635	7.7	16.3	6.85	0.477	0.0098	9.97	1.838	Number of layers: 3, class: 4th [19]
	S. D	42	0.7	4.1	0.96	0.147	0.0063	1.25	0.433	
PB	Ave	761	10.4	11.0	3.60	1.566	0.0273			Use: structural, bending class: 18N/mm² [16]
	S. D	14	0.9	1.2	0.43	0.269	0.0048			
MDF	Ave	820	7.2	26.1	3.98	1.622	0.0285			Use: structural, bending class: 30N/mm² [17] forming: dry forming
	S. D	17	0.4	1.1	0.15	0.280	0.0088			
HB	Ave	1008	8.6	25.0	5.51	1.032	0.0135			Bending class: 35N/mm² [17] forming: wet forming
	S. D	86	0.2	1.6	0.82	0.214	0.0042			

Ave. means average, and S. D. means standard deviation. Three mechanical tests were conducted according to ASTM D 1037 [20]

Sudo *et al. Journal of Wood Science*   (2023) 69:18

Page 4 of 15

parameters used in the tests were the dowel diameter, pilot hole diameter, end distance, and edge distance. First, the failure process was observed closely, and the effects of the parameters on the failure mode were verified. Second, based on the obtained results, the yield stress, maximum stress, and ultimate displacement (ductility) were calculated, and the relationship between ductility and parameters was verified. Finally, a standardized multiple regression analysis (SMRA) was performed to quantitatively analyze the influence degree of various conditions on each characteristic value.

Materials and methods
Specimens
The panel types used in the test were PW, OSB, PB, MDF, and HB. The fundamental properties of these panels, including the density, moisture contents, tensile and in-plane shear strength, and some information regarding standard classification, are shown in Table 1. An in-plane shear test was conducted on only the orthotropic panels (PW and OSB), i.e., not on the isotropic panels (PB, MDF, and HB). As PW and OSB are in-plane orthotropic materials, the embedment test was conducted along both strong and weak axes (a strong (weak) axis specification implies that the load is parallel (perpendicular) to the fiber on the surface layer). In addition, a trailing "-s" (e.g., PW-s) indicates the strong axis, whereas a trailing "-w" (e.g., PW-w) indicates the weak axis. The thickness of the HB specimen was 5 mm, whereas that of the other panel types was 9 mm.

The other parameters were set as follows: the dowel diameter d (5.2 and 12 mm), the dowel position (from A to G, as shown in Fig. 1), and the pilot hole size ph (0, 1/3, 2/3, and 1 times the diameter). The combination of the dowel position and ph is shown in Fig. 1 as well. For the dowels, an N150 nail ($d = 5.2$ mm, defined by JIS [32]) and a custom-developed dowel ($d = 12$ mm) were used, as shown in Fig. 2. Tests based on 44 specifications were conducted for each panel type, and the number of specimens was six per specification. However, the embedment test could not be conducted on some PB and MDF specimens because they were fractured during nailing prior to the test. In particular, at the dowel position F and $d = 5.2$ mm, all specimens were fractured except when $ph = 1$.

Test methods
Embedment tests were conducted by applying a tensile force through a sandwich structure comprising a pair of steel plates with a rectangular hole (see Fig. 3). A jig was designed to enable the observation of the failure process and eliminate the depth clearance. The specimen panel with a dowel inserted was set on the lower section of the jig, and the lower section of the panel was fixed by clamping. At the upper section of the jig, a panel with a thickness equal to that of the specimen was inserted and tightened loosely with two M20 bolts. The upper side of this panel was clamped and pulled up. Because the dowels used for the specimen were less than 20 mm in terms of their diameter, i.e., 5.2 and 12 mm, only they were embedded in the specimen, whereas the M20 bolts were only slightly embedded into the other panel. A monotonic tensile load was applied to the specimen at 3 and 4 mm/min ($d = 5.2$ mm) or at 6 and 7 mm/min ($d = 12$ mm). Both test speeds can be regarded as static speeds, and the difference in the test speeds can be assumed to impose no effect on the test results. The absolute deformation was measured using four displacement transducers placed at the corners of the jig, and the average deformation was regarded as the entire deformation. The test was continued until the specimen fractured completely. After the test was completed, the dowel did not exhibit any bending deformation.

Results and discussion
Failure mode
Based on the embedment test, two failure modes were observed: one was shear failure at the area above the dowel, as shown in Fig. 4, hereafter termed "end shear failure (ESF)," and the other was tensile failure at the area next to the dowel, as shown in Fig. 5, hereafter termed "side tensile failure (STF)." ESF constitutes ductile failure, whereas STF constitutes brittle failure. STF occurred only at dowel positions D to G. In addition, partial buckling failure occurred in PW-w and OSB-w when the dowel position was F (see Fig. 6). However, the tendency of partial buckling failure, such as the high probability of occurrence with the narrow edge distance and its brittleness, were similar to those of STF, and this failure behavior was classified as STF in this study to simplify the discussion.

The STF resembled simple tensile failure and did not differ significantly among the panel types. Moreover, the ESF showed some differences among the panel types. Figure 7 shows a summary of the fracture progression during the test and the failure appearance of each panel after the test. In this figure, all parameters except the panel type are standardized uniformly (dowel position: A, d: 12 mm, ph: 1).

The ESF mode exhibited two types of failure behavior: a crack on the surface of the panel generated by in-plane tensile or shear stress, termed "in-plane failure," and a peeled surface divided into several layers. Peeled surface failure is generated by the Poisson effect of the compressive stress immediately above the dowel and is termed "out-of-plane failure."
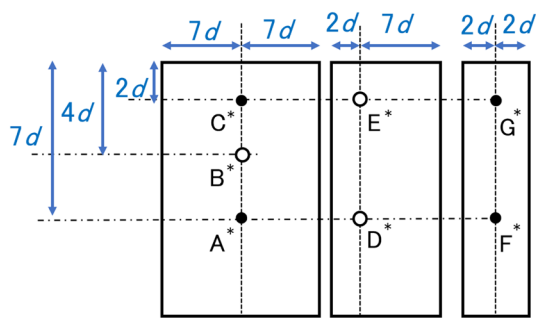
* Label for the dowel position.

Fig. 1 Combination of the dowel position and *ph*. * Label for the dowel position. Four tests of *ph* (i.e., 0, 1/3, 2/3, and 1) were conducted at the dowel positions indicated by black circles. Two tests of *ph* (0, 1) were conducted at the white circled dowel positions. *d* and *ph* mean the dowel diameter and the pilot hole size, respectively
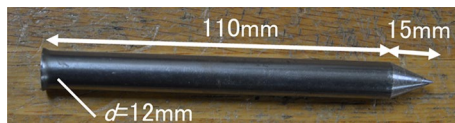
Fig. 2 Schematic illustration of the 12 mm pin

Although these two types of failure behavior generally occurred simultaneously, it was possible to identify the dominant failure behavior for each panel type.

After the test was completed, vertical and horizontal crack lines were observed in PW-s and PW-w, respectively. Although the layers of the specimens were separated after the test, they were only slightly delaminated. This separation of layers was caused by the difference in failure mode in the fiber direction of the veneer, not by the Poisson effect.

Compared with the PW specimen, the OSB specimen did not show a clear crack line. Additionally, the surface layer of the OSB specimen peeled off more significantly than that of the PW specimen. Therefore, based on a comparison between the PW and OSB specimens, in-plane failure and out-of-plane failure were dominant in the former and latter, respectively.

For the PB, horizontal tensile failure occurred immediately above the dowel after the test was completed. Layer separation was not observed.

Similar to the PB results, horizontal tensile failure occurred immediately above the dowel in the MDF. However, the photograph shown in Fig. 7 (captured from the upper angle) shows a failure mode where the panel was separated into two layers (in some specimens, into three layers), which was not observed in the PB.

Moreover, the HB panel fractured by peeling, as similarly observed in the OSB. The photograph in Fig. 7

(captured from the upper angle) shows a failure mode where the panel was separated into several layers.

Based on a comparison of the three isotropic materials, the dominant failures exhibited by the PB, HB, and MDF were in-plane failure, out-of-plane failure, and a failure mode between in-plane and out-of-plane failure, respectively.

To correlate these failure behaviors with the material property, the "in-to-out plane strength," which is defined by the tensile strength divided by the internal bond strength, was introduced. The in-to-out plane strengths of the PW, OSB, PB, MDF, and HB were 14.6, 34.6, 7.00, 16.06, and 24.17, respectively.

A comparison of the in-to-out plane strength of the orthotropic panels shows that a panel with a higher in-to-out plane strength is dominated by out-of-plane failure. The fracture mechanism is shown in Fig. 8. The same trend was observed for the isotropic panels. These results suggest that the in-to-out plane strength is related to the failure behavior under the embedment pressure.

The OSB and HB specimen exhibited the highest in-to-out plane strength ratios among the in-plane orthotropic and in-plane isotropic panels, respectively. In these panels, the final failure was due to peeling, which resulted in a slower load reduction at the failure point, as further discussed in the subsequent sections.

Next, a discussion regarding the STF is presented. Table 2 lists the number of specimens undergoing STF at positions D to G.

First, for all panel types, STF was more likely to occur at D than at E and at F than at G. This might be because specifications involving a short end distance are more likely to be fractured via ESF than via STF.

STF tended to occur more frequently in the 5.2 mm nail than in the 12 mm dowel (see Table 2). According to previous studies regarding the lateral embedment of timber [33, 34], stress spreading ranges are absolute ranges. In other words, they are not determined by the pressure area. The length of the edge distance was set based on the diameter in this test; hence, the spreading range of horizontal stress of the 5.2 mm nail was relatively wider than that of the 12 mm dowel. This difference in the relative spreading range of horizontal stress might have contributed to the test result mentioned above.

Additionally, STF tended to occur more in the loading of the weak axis than that of the strong axis. The STF was similar to simple tensile failure; therefore, pure tensile strength was assumed to have contributed to the failure mode.

Derivation method of the characteristic values

Stress was calculated by dividing the load by the projection area of the dowel, after which the

Sudo *et al. Journal of Wood Science*   (2023) 69:18

Page 6 of 15
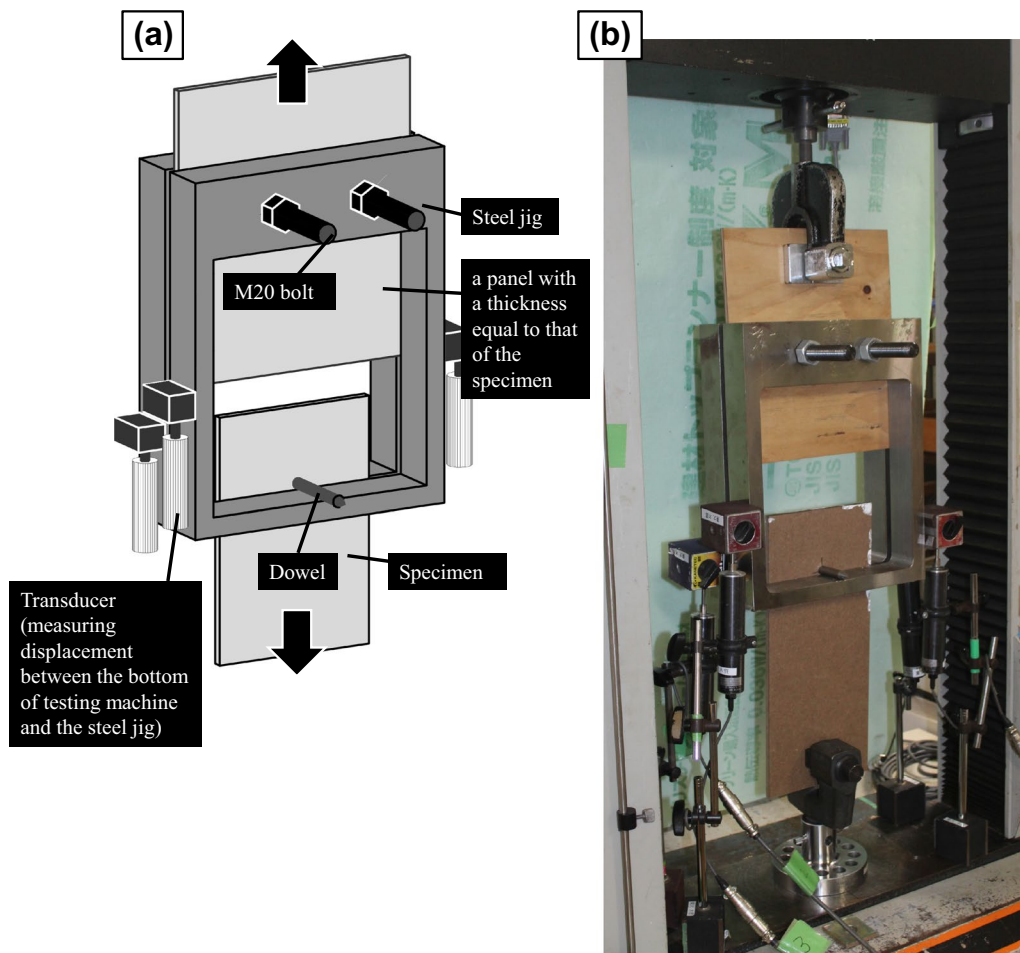
Fig. 3 Schematic illustration of the embedment test. **a** Schematic illustration of the test setup; **b** photograph of the test setup (panel = MDF, d = 12 mm, ph = 1, and dowel position = A)


Fig. 4 End shear failure (ESF). The parameters were as follows: panel type, PW-s; d, 5.2 mm; ph, 0; dowel position, A

stress–displacement curves were obtained. Based on these displacement curves, the maximum stress σ_{max} (MPa), yield stress σ_{y} (MPa), and ultimate displacement u (mm) were derived using the method presented next.

A simple illustration of the method is shown in Fig. 9. Some of the stress–displacement curves included load recovery. In this study, once the stress decreased to 80% of the previous maximum stress, the first peak was considered σ_{max}, even when the maximum stress was updated after load recovery. In this study, u was defined as the displacement at 80% of the maximum stress of the entire stress–displacement curve ($\sigma_{max\text{-}sub}$ in Fig. 9), including after load recovery. Moreover, σ_{y} was derived via the 5%-offset method using a linear elastic line in the linear range (i.e., offset the length to equal to 5% of the dowel diameter). This line was derived from the points at 20% and 50% of σ_{max}. However, there were a few specimens where a clear reduction in stiffness was observed at values below 50% of the maximum stress.
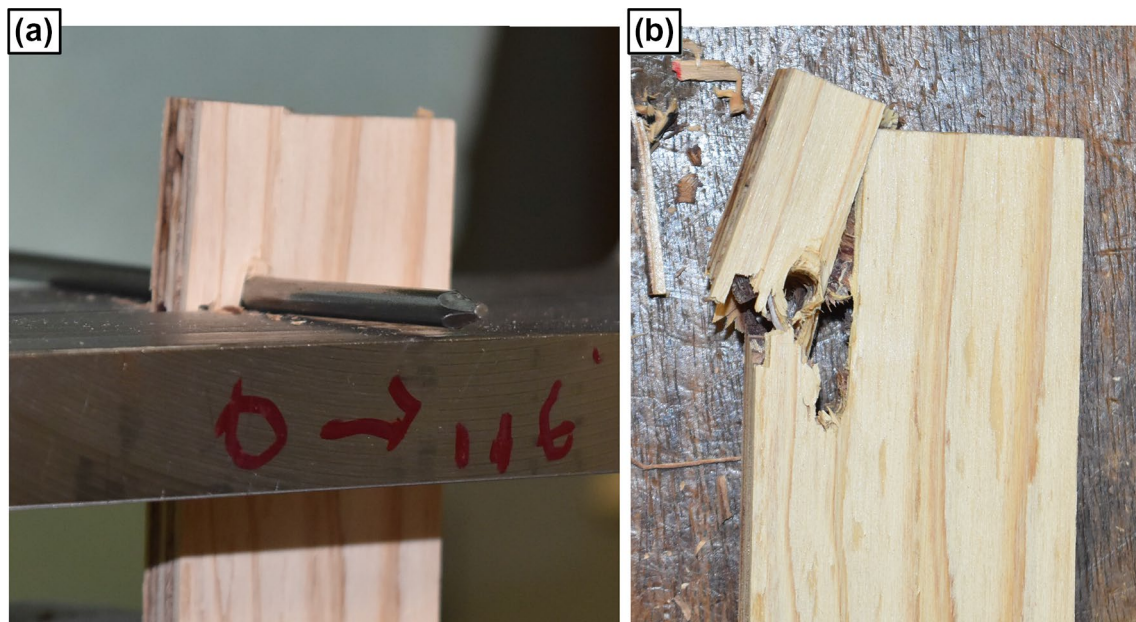
Fig. 5 Side tensile failure (STF). **a** just after failure and **b** after removal from the jig. The parameters were as follows: panel type, PW-s; *d*, 5.2 mm; *ph*, 1; dowel position, D
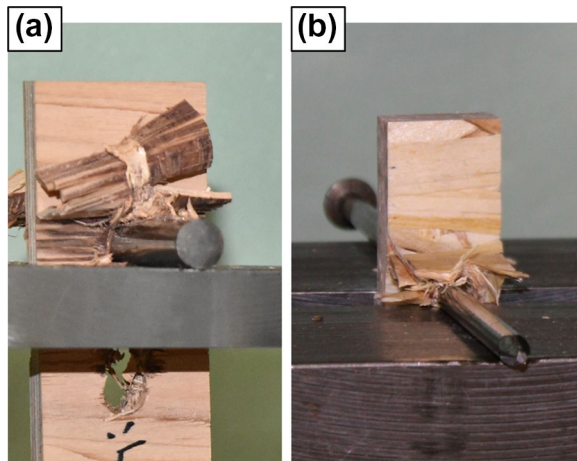
Fig. 6 Partial buckling failure. **a** PW-w and **b** OSB-w. The other parameters for PW-w were as follows: *d* = 12 mm, *ph* = 1/3, and dowel position = F. The other parameters for OSB-w were as follows: *d* = 5.2 mm, *ph* = 0, and dowel position = F

For these specimens, normal evaluation of the characteristic values was impossible. In this case, a range within the linear range was determined for each specimen. Additionally, based on the cases where the STF occurred, the STF was shown to constitute brittle failure, and the intersection between its curve and the offset line typically occurred after σ_{max}. In this case, σ_{max} was regarded as σ_y.

Comparison of ductility

The ultimate displacement is typically used to compare ductility. However, as the ultimate displacement measured in this study was significantly affected by the original end distance, it was not regarded as an appropriate indicator of ductility. Additionally, the original end distance was set based on *d*, and *u* is also affected by *d*. Hence, the remaining distance (*RD*) was introduced. *RD* is expressed in Eq. 1.
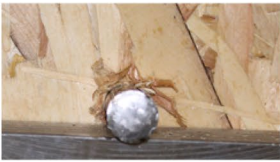
$$RD = \frac{e_{origin} - u}{d} \tag{1}$$

where e_{origin} is the original end distance. For example, e_{origin} equals 36.4 mm when $d = 5.2$ at dowel position A.

Figure 10 shows a comparison of the *RD* values. The smaller *RD* is, the higher the ductility.

The trends observed in all the panel types were as follows: (1) *RD* of A and B was similar, (2) the average values of *RD* at D or F and their standard deviations were higher than those at any other dowel positions, and (3) *RD* for $d = 5.2$ mm was typically higher than that for $d = 12$ mm.

First, the average values of *RD* of A and B were similar, i.e., from 2 to 4. In other words, *u* at the dowel position of A ranged from 15.6 mm to 26 when $d = 5.2$ mm and from 36 to 60 mm when $d = 12$ mm. For the embedment of timber, if the ratio of the thickness to *d* is low and dowel bending is not observed, then brittle splitting typically occurs [35]. From the test results, it

Sudo *et al. Journal of Wood Science*   (2023) 69:18

Page 8 of 15

	During the test (front view)	After the test (front view)	After the test (top view)
PW-s			
PW-w			
OSB-s			
OSB-w			
PB			
MDF			
HB			

**Fig. 7** Comparison of ESF behavior among panel types
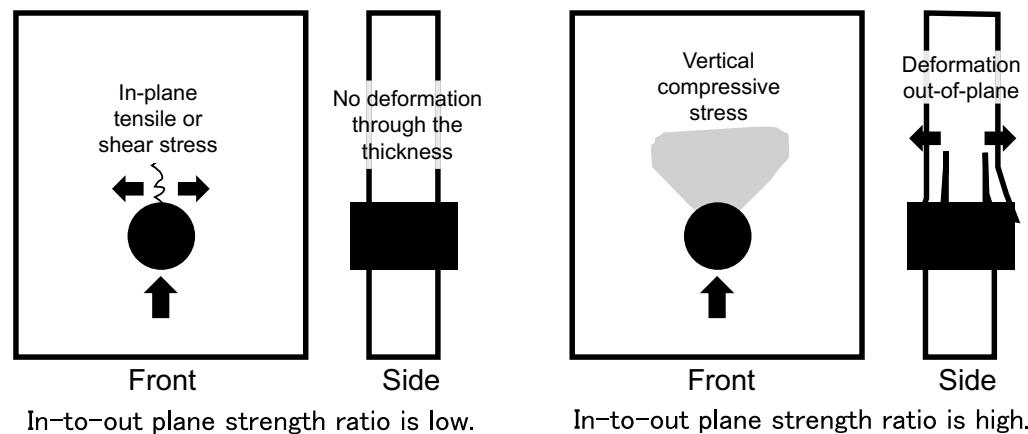
Fig. 8 Two fracture processes of the ESF

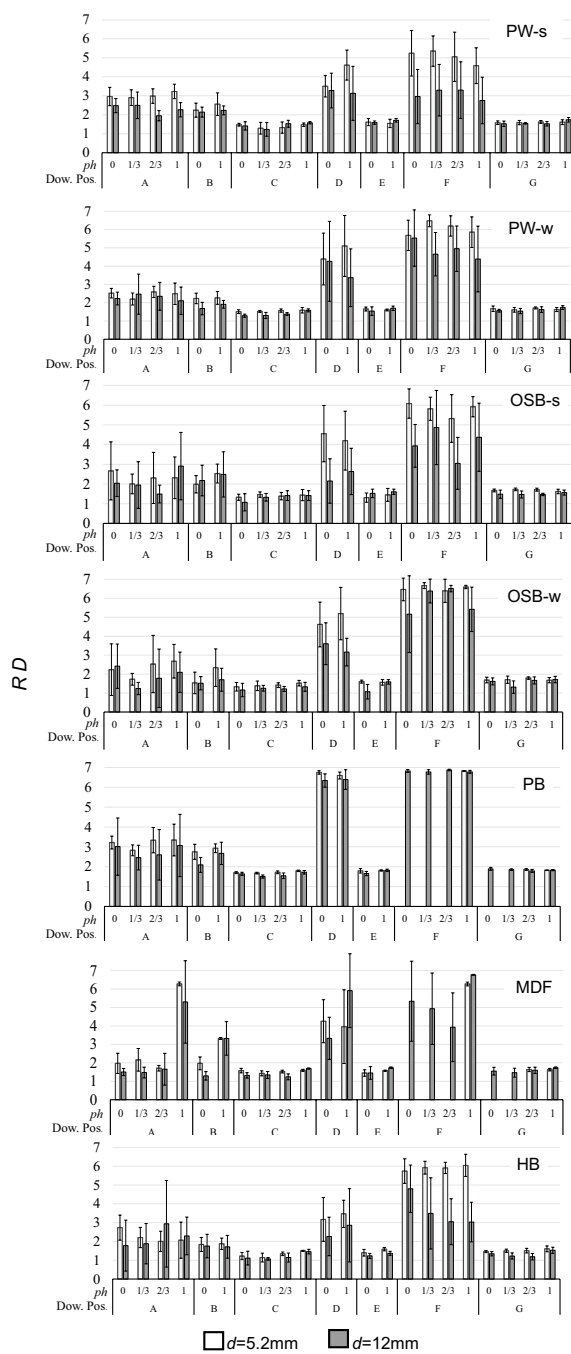**Table 2** Number of specimens where STF occurred

Dowel position	ph	PW-s		PW-w		OSB-s		OSB-w		PB		MDF		HB	
		d=5.2	d=12	d=5.2	d=12	d=5.2	d=12	d=5.2	d=12	d=5.2	d=12	d=5.2	d=12	d=5.2	d=12
D	0	3	2	5	3	3	2	5	4	6	6	5	3***	4	0
	1	4	1	5	2	5	1	6	5	6	6	0	0	3	1
E	0	3	3	5	4	1	1	4	3	5	3	0	0**	0	0
	1	4	0	5	4	1	2	2	3	3	1	1	0	0	0
F	0	3	3	6	0	6	4	6	5	None*	6	None*	5	6	4
	1/3	4	2	6	5	6	3	6	6	None*	6	None*	4	6	3
	2/3	5	2	6	4	4	3	6	6	None*	6	None*	2	6	5
	1	4	0	6	5	6	5	6	6	6	6	6	3	6	5
G	0	3	4	5	4	6	2	5	5	None*	4	None*	3	5	0
	1/3	3	2	5	4	5	3	5	6	None*	5	None*	3	3	0
	2/3	1	1	5	4	5	2	6	5	6	4	5**	3	1	1
	1	2	0	3	3	6	0	6	4	4	6	2	2	0	0

* All specimens were fractured during nailing. **One specimen out of six was fractured during nailing. ***Two specimens out of six were fractured during nailing

d and *ph* mean the dowel diameter and the pilot hole size, respectively
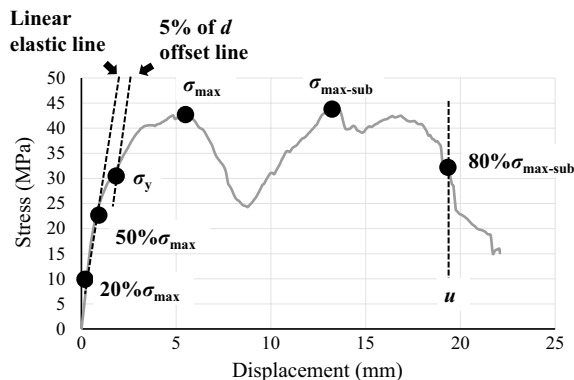
Fig. 9 Evaluation of characteristic values based on the stress–displacement curve. The parameters of the specimen were as follows: panel type, PW-s; *d*, 5.2 mm; *ph*, 0; and dowel position, A
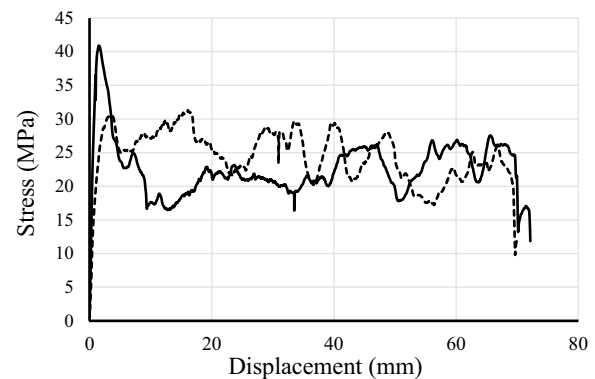
became clear for the embedment of wood-based panels that when the edge distance was sufficient, the failure mode was ductile, and the load did not decrease until the remaining end distance reached a certain value. This implies that the prevalent belief for timber is not valid for wood-based structural panels. This mechanism is independent of the original end distance. However, for the MDF, when the dowel position was A and *ph* was 1, the *RD* values were high, and hence, the ductility was low. An example of the stress displacement curves is shown in Fig. 11. Based on this figure, the evaluated ductility is low because the specimen reached the maximum stress early and then maintained 50%–60% of the maximum stress. In this study, *u* was defined as the displacement at 80% of the maximum stress. Hence, *u* is

Sudo *et al. Journal of Wood Science*   (2023) 69:18

Page 10 of 15

Fig. 10 Comparison of *RD* values. Dow. Pos. indicates the dowel position. Error bars indicate standard deviation

Fig. 11 Comparison of stress–displacement curves of MDF for different *ph values*. The solid curve is the stress–displacement curve when *ph* = 1 and the dotted curve when *ph* = 0. The other parameters were as follows: *d* = 12 mm and dowel position = A

dowel positions. As described previously, the failure mode at dowel position D or F was STF in some cases and brittle. Consequently, the values of *RD* at D and F were high. In addition, a mixture of failures involving both ESF and STF occurred in the same specification, which resulted in a significant variation in *RD*. However, for the PB, the standard deviation was low because all specimens fractured via STF.

Third, *RD* for *d* = 5.2 mm was higher than that for *d* = 12 mm. As described above, the relative spreading range of the horizontal stress, which was standardized by *d*, was assumed to be larger when *d* = 5.2 mm in comparison with *d* = 12 mm. Therefore, the results at positions D–G, where STF is likely, can be interpreted as in the previous section on "comparison of ductility". Although ESF occurred at dowel positions A–C, the same interpretation can be used to explain these results, assuming the spreading range of the vertical relative stress was also larger when *d* = 5.2 mm. Therefore, this suggests that the relative stress spreading range was larger both horizontally and vertically when *d* = 5.2 mm in comparison with *d* = 12 mm.

Additionally, the standard deviations of the OSB and HB were higher than those of the other types of panels at position A. The stress–displacement curves of some panel types at A are shown in Fig. 12. The two panels mentioned above exhibited a high in-to-out plane strength ratio and ultimately fractured by the peeling of the surface layer, as mentioned in the previous section. The panels that fractured based on this mechanism exhibited a slower load decrease, thus resulting in an *RD* value with a high standard deviation.

A comparison of the *RD* values based on the calculated "strong axis specification—weak axis specification" values for the PW and OSB are shown in Fig. 13.

evaluated just after the point of the maximum stress in this case. Conversely, the typical case, depicted as the dotted line (*ph* = 0) in Fig. 11, exhibits a stress retention of 60–90%, with the ultimate displacement deemed evaluated appropriately.

Second, the average values of *RD* at D or F and their standard deviations were higher than those at any other
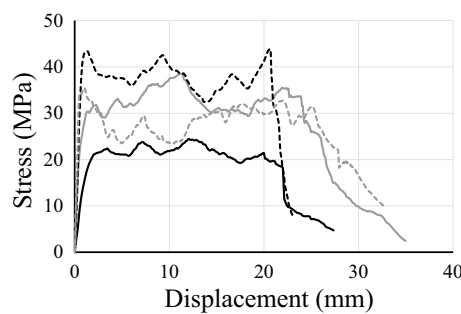
Sudo *et al. Journal of Wood Science* (2023) 69:18

Page 11 of 15

Fig. 12 Comparison of stress–displacement curves among panel types. The black solid curve is the stress–displacement curve for PW-s, black dotted curve for PB, gray solid curve for OSB-s, and gray dotted curve for HB. The other parameters were as follows: $d = 5.2$ mm; $ph = 1$; dowel position $= A$

The values were positive at positions A–C and negative at positions D and F for both the PW and OSB. Along the weak axis, STF occurred more frequently, and *RD* was higher, as described above. Therefore, the values were negative at positions D and F. To account for the results at positions A–C, it is necessary to assume that the vertical stress spreading range is important for *RD* when ESF occurs and that the vertical stress spreading range is larger along the strong axis. This makes it easier for stress to reach the top end and causes earlier fracture of the strong axis. These results suggest that the stress spreading range of the strong axis was larger vertically and smaller horizontally than that of the weak axis. However, this could not be confirmed experimentally, necessitating further study.

SMRA method

To quantitatively verify how much each parameter had an influence on each characteristic value, SMRA was conducted.

The characteristic values with five explanatory variables are expressed in Eq. 2.

$$y = \sum_{i=1}^{5} a_i x_i + \epsilon \tag{2}$$

where y is the objective variable, x_i is the explanatory variable, a_i is its partial regression coefficient, and ε is the error.

Five explanatory variables were set as follows: dowel diameter d (mm), ratio of the pilot hole *ph*, ratio of the end distance to the diameter e, variable *side2* that equals 1 when the dowel position was D or E and 0 otherwise, and variable *side3* that equals 1 when the dowel position was F or G and 0 otherwise. Additionally, σ_{max} and σ_y were set as the objective variables. Each variable was standardized to have a mean of 0 and standard deviation of 1 using Eq. 3 before analysis.

$$\bar{p} = \frac{p - \sigma}{s} \tag{3}$$

where p is the original value, $\bar{p}$ is the standardized value, σ is the average value, and s is the standard deviation.

Supposing that the variable with the upper line indicates that it has been standardized, Eq. 2 can be rewritten as in Eq. 4.

$$\bar{y} = \sum_{i=1}^{5} a_i \overline{x_i} + \epsilon \tag{4}$$

Some specimens were fractured during nailing before the test was performed, as described previously; therefore, those specimens were not included in the target of the SMRA.

The partial regression coefficients are representative of the influence degree of the parameter on the characteristic value. Therefore, this value can reveal the dominant influencing factor.

Results of SMRA coefficients

The SMRA results are shown in Table 3. The table shows that the p value is below 0.05 if the partial regression coefficient exceeds 0.1 or is less than −0.1.
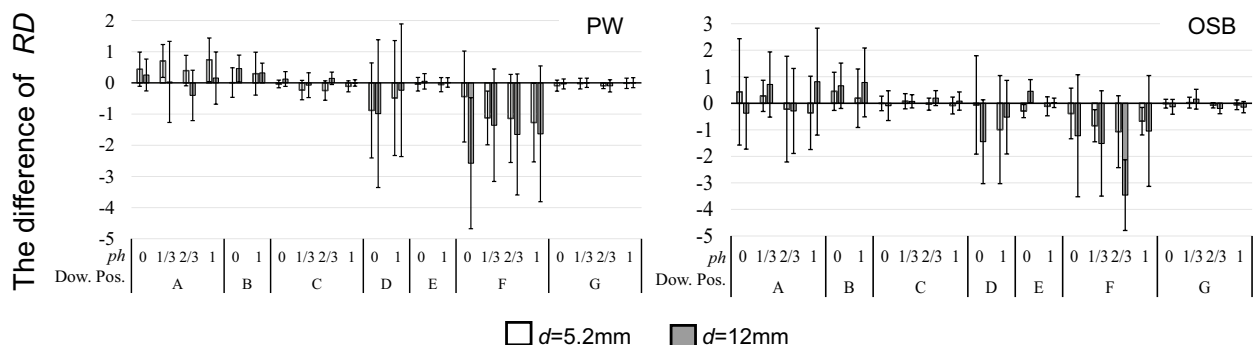

Fig. 13 Comparison of *RD* differences between strong and weak axial specifications. Values of "strong axial specification—weak axial specification" are presented. Error bars indicate standard deviation

Sudo *et al. Journal of Wood Science*   (2023) 69:18

Page 12 of 15

Table 3 Values of the partial regression coefficient

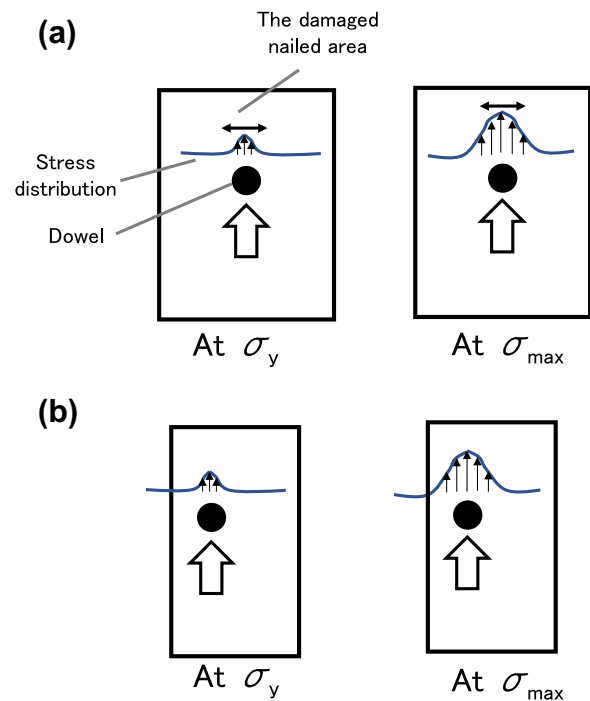|		PW-s	PW-w	OSB-s	OSB-w	PB	MDF	HB
$a_{\overline{d}}$	σ_y	**−0.31**	**−0.34**	**−0.44**	**−0.44**	**−0.28**	**−0.46**	**−0.39**
	σ_{max}	**−0.32**	**−0.36**	**−0.56**	**−0.44**	**−0.29**	**−0.51**	**−0.49**
$a_{\overline{ph}}$	σ_y	**0.23**	**0.32**	**0.33**	**0.42**	**0.50**	**0.64**	**0.41**
	σ_{max}	0.03	0.05	**0.19**	**0.20**	**0.33**	**0.56**	**0.10**
$a_{\overline{e}}$	σ_y	**0.54**	**0.34**	**0.19**	0.08	**0.21**	**0.11**	**0.16**
	σ_{max}	**0.74**	**0.57**	**0.38**	**0.28**	**0.37**	**0.20**	**0.37**
$a_{\overline{side2}}$	σ_y	0.08	**−0.11**	0.03	0.07	**−0.10**	**0.11**	**0.25**
	σ_{max}	−0.02	**−0.21**	−0.08	−0.08	**−0.21**	**0.10**	**0.18**
$a_{\overline{side3}}$	σ_y	−0.08	**−0.38**	−0.08	**−0.31**	**−0.49**	−0.02	−0.07
	σ_{max}	**−0.12**	**−0.43**	**−0.21**	**−0.40**	**−0.57**	−0.04	**−0.20**

Bold number indicates that the *p* value is under 0.05. σ_y and σ_{max} mean the yield stress and the maximum stress, respectively
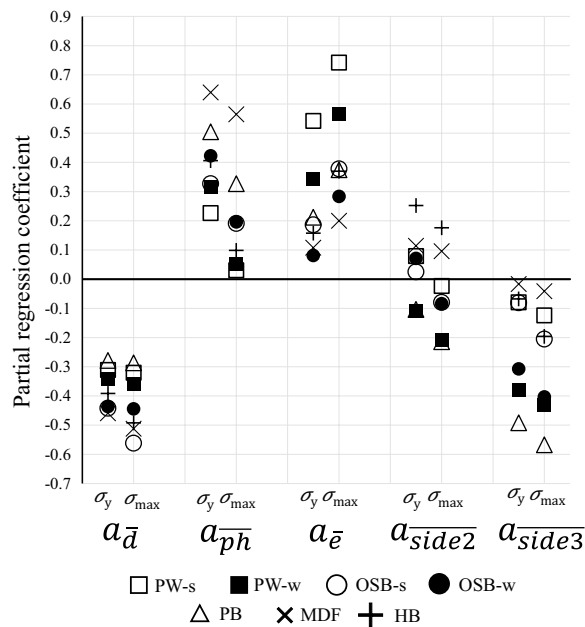
Fig. 14 Comparison of partial regression coefficients. $a_{\overline{d}}$, $a_{\overline{ph}}$, $a_{\overline{e}}$, $a_{\overline{side2}}$ and $a_{\overline{side3}}$ mean partial regression coefficients of $\overline{d}$, $\overline{ph}$, $\overline{e}$, $\overline{side2}$ and $\overline{side3}$ in Eq. 4, respectively

Fig. 15 Influence of the widened stress spreading range. **a** is an illustration demonstrating that *ph* had a stronger influence on σ_y than on σ_{max}. **b** is an illustration demonstrating that the dowel position had a stronger influence on σ_{max} than on σ_y

A comparison of the values of the partial regression coefficient is shown in Fig. 14.

As shown in Fig. 14 and Table 3, the overall results of σ_y and σ_{max} are approximately the same, but the dispersion varies. Figure 14 and Table 3 indicate that *ph* had a stronger influence on σ_y than on σ_{max}. They also indicate that *e*, *side2*, and *side3* had a stronger influence on σ_{max} than on σ_y. These results can be interpreted consistently by assuming that the stress spreading range increased at σ_{max} in comparison to that at σ_y by stress redistribution. Based on this assumption, as shown in Fig. 15a, the damaged nailed area, which was assumed to grow as *ph* decreased, was not small enough to ignore at σ_y; the stress spreading range widened at σ_{max}, and the damaged area narrowed relatively. As a result, *ph* had a stronger influence on σ_y than on σ_{max}. Similarly, as shown in Fig. 15b, even when the end or edge space was narrow, it had no effect on σ_y because the stress spreading range at σ_y was also small. However, when the stress spreading range widened to some extent at σ_{max}, the range reached the edge and affected the strength. Consequently, the coefficients for σ_y and σ_{max} differed.

However, this cannot be confirmed experimentally, and further investigations are needed.

An analysis of the $a_{\bar{e}}$ of $\sigma_{\max}$ suggests that e exerted the strongest influence on the $\sigma_{\max}$ of the PW and a stronger influence on the $\sigma_{\max}$ of the strong axis of the PW and OSB than on their weak axis. As described previously regarding RD, the strong axis exhibited a lower ductility than the weak axis when ESF occurred. This is assumely attributable to the larger spread range of vertical stress along the strong axis. Based on this assumption, the $\sigma_{\max}$ of the strong specification is certainly affected by e. Similarly, the spread range of the vertical stress of the PW is the largest among all the panel types. However, these conjectures are not confirmed, and further investigations are necessary.

Based on a comparison between $a_{\overline{side2}}$ and $a_{\overline{side3}}$, the overall trends were similar, and the absolute value of $a_{\overline{side3}}$ was larger than that of $a_{\overline{side2}}$. Additionally, the values of $a_{\overline{side2}}$ and $a_{\overline{side3}}$ of $\sigma_{\max}$ were strongly negative for PW-w, OSB-w, and PB. In general, a large stress spreads horizontally when a compressive stress is applied in the direction perpendicular to the grain, and the spreading of this stress contributes to the strength [33, 34]. Therefore, it is natural that the weak axis was highly influenced by the edge distance. Moreover, the PB had low ductility, and STF tended to occur when the dowel position was D or F in Table 2. Therefore, the PB strength was assumely susceptible to the horizontal stress spread, and these results were consistent.

Conclusion

To obtain the embedment properties of wood-based structural panels, an embedment test was conducted for specimens PW, OSB, PB, MDF, and HB. Both strong and weak axes of the PW and OSB were tested. The dowel diameter, pilot hole size, end distance, and edge distance were regarded as the test parameters. The effects of these parameters on each of the embedment properties, i.e., the failure mode, ductility, yield stress, and maximum stress, were discussed.

The following findings were obtained regarding the failure mode:

- The two main failure modes observed in the tests were ESF with sufficient edge distance and STF with insufficient edge distance.
- In terms of the ESF mode, peeling of the surface layer dominated the HB and OSB specimens, whereas in-plane tensile or shear failure dominated the PW and PB specimens.
- The weak axis was more likely to exhibit STF than the strong axis specification.

- In terms of ductility, the following findings were obtained:
- When the edge distance was sufficient, the failure mode was ductile; additionally, the load did not decrease until the remaining end distance reached a certain value.
- When STF occurred, the ductility was low.
- The ductility was higher at larger dowel diameters.
- The ductility along the strong axis was lower than that along the weak axis when ESF occurred. When STF occurred, the opposite trend was observed.
- The effects of the parameters on σ_y and $\sigma_{\max}$ were analyzed via SMRA, and the main findings were as follows:
- The overall results of $\sigma_{\max}$ and σ_y were approximately the same; however, the pilot hole affected σ_y more significantly than it did $\sigma_{\max}$, whereas the opposite was observed for the end and edge distances.
- A decrease in the embedment strength owing to the insufficient end distance length was evident in the PW, particularly for the strong axis.
- A decrease in the embedment strength owing to the insufficient edge distance length was evident in the PB and in the PW and OSB for the weak axis.
- Some assumptions introduced to explain these results were as follows:
- The ratio of the in-plane tensile strength to the internal bond strength determines the final failure behavior.
- The relative stress spread range is smaller when the dowel diameter is larger.
- The relative stress spread range is larger at the maximum stress than at the yield stress.
- The stress generated by the embedment pressure is more likely to spread vertically and horizontally in the strong and weak axes, respectively.

These assumptions cannot be verified completely based only on the current study; hence, further investigations are needed. However, this paper is the first to comprehensively and systematically discuss the embedment properties of wood-based structural panels. The findings presented herein are expected to contribute to the diversification of structural designs based on wood-based structural panels and to facilitate the development of new panels.

Abbreviations

PW	Plywood
OSB	Oriented strand board
PB	Particleboard
MDF	Medium density fiberboard
HB	Hardboard
JIS	Japanese Industrial Standards

Sudo *et al. Journal of Wood Science*   (2023) 69:18

Page 14 of 15

JAS   Japanese Agricultural Standards
ASTM   American society of testing and material
SMRA   Standardized multiple regression analysis
STF   Side tensile failure
ESF   End shear failure

Availability of data and materials
The datasets used and analyzed in the current study are available from the corresponding author upon reasonable request.

Declarations

Competing interests
The authors declare that they have no competing interests.

References

1. Thoemen H, Irle M, Sernek (eds) (2016). COST, London
2. Johansen KW (1949) Theory of timber connections. Int Assoc Bridge Struct Eng 9(1949):249–262
3. Kuenzi EW (1955) Theoretical design of a nailed or bolted joint under lateral load. Forest Products Laboratory Report: No. 1951
4. Sawata K, Yasumura M (2002) Determination of embedding strength of wood for dowel-type fasteners. J Wood Sci 48:138–146
5. Hwang H, Komatsu K (2002) Bearing properties of engineered wood products I: effects of dowel diameter and loading direction. J Wood Sci 48:295–301
6. Wakashima Y, Hirai T (1996) Nail-wood bearing properties.1. Effects of initial gripped conditions of nails driven into wood. Mokuzaigakkashi 42(6):574–580
7. Nakagomi T, Kambe W, Ikura Y (2009) A study with fracture mechanics on evaluation of strength and fracture characteristics for bolted joints with Japanese larch glulam tensile loaded perpendicular to grain. J Struct Eng (AIJ) 74(643):1649–1658. https://doi.org/10.3130/aijs.74.1649
8. Van der Put TACM, Leijten AJM (2000) Evaluation of perpendicular to grain failure of beams caused by concentrated loads of joints. Proceedings of the international council for research and innovation in building and construction, CIB-W18 Meeting Thirty-Three, Delft, The Netherlands, paper no. 33-7-7
9. Kuwamura H (2013) Fracture modes of wood in single-bolted joints loaded parallel to grain—study on steel-framed timber structures part 15. J Struct Eng (AIJ) 78(685):529–538. https://doi.org/10.3130/aijs.78.529
10. Racher P, Bocquet JF (2005) Non-linear analysis of dowelled timber connections: a new approach for embedding modelling. Electro J of Struct Eng 5:1–9
11. Sjödin J, Serrano E, Enquist B (2008) An experimental and numerical study of the effect of friction in single dowel joints. Holz Roh Werkst 66:363–372. https://doi.org/10.1007/s00107-008-0267-z
12. Schoenmakers (Dennis) JCM, Svensson S (2011) Embedment tests perpendicular to the grain—optical measurements of deformation fields. Dig Eur J Wood Wood Prod. https://doi.org/10.1007/s00107-008-0267-z
13. Lederer W, Bader TK, Muszyński L, Eberhardsteiner J (2016) Exploring a multi-modal experimental approach to investigation of local embedment behaviour of wood under steel dowels. Strain 52:531–547. https://doi.org/10.1111/str.12199
14. HONG J (2007) Three-dimensional nonlinear finite element model for single and multiple dowel-type wood connections. Dissertation, University of British Columbia
15. Sandhaas C, Sarnaghi AK, van de Kuilen JW (2020) Numerical modelling of timber and timber joints: computational aspects. Wood Sci Technol 54:31–61. https://doi.org/10.1007/s00226-019-01142-8
16. Japanese Industrial Standards (2015) JIS A 5908 Particleboards. Japanese Standards Association, Tokyo
17. Japanese Industrial Standards (2014) JIS A 5905 Fiberboards. Japanese Standards Association, Tokyo
18. Japanese Agricultural Standard (2014) JAS for plywood. Japanese Agricultural Standards Association, Tokyo
19. Japanese Agricultural Standard (2013) JAS for OSB. Japanese Agricultural Standards Association, Tokyo
20. AST D1037-12 (2017) Standard test method for evaluating properties wood-based fiber and particle panel materials. ASTM International, West Conshohocken, PA
21. Sekino N, Morisaki S (1987) The effects of board density and board-edge distance of nails on lateral nail-resistance of low-density particleboards. Mokuzaigakkaishi 33(9):694–701
22. Sekino N, Seino M (2015) Effects of test methods on lateral nail resistance of particleboards. Mokuzaigakkaishi 61(1):40–47. https://doi.org/10.2488/jwrs.61.40
23. Van der Put TACM (2008) Explanation of the embedding strength of particle board. Eur J of Wood and Wood Products 66(4):259–265. https://doi.org/10.1007/s00107-008-0234-8
24. Sekino N, Sato H, Adachi K (2014) Evaluation of particleboard deterioration under outdoor exposure using several different types of weathering intensity. J Wood Sci 60:141–151. https://doi.org/10.1007/s10086-013-1384-9
25. Korai H, Fujimoto Y (2015) Nail-head pull-through strength and lateral nail resistance strength of wood-based boards subjected to various climatic conditions in Japan. J Wood Sci 61:401–411. https://doi.org/10.1007/s10086-015-1485-8
26. Kojima Y, Kobayashi C, Shoji T, Kobori H, Suzuki S, Nishikido K, Takahashi K (2019) Effect of accelerated aging test condition on the nailed joint performance of wood-based panels for construction. Mokuzaigakkaishi 65(1):39–45. https://doi.org/10.2488/jwrs.65.39
27. Sawata K, Shibusawa T, Ohashi K, Castellanos SRJ, Hatano Y (2008) Effects of density profile of MDF on stiffness and strength of nailed joints. J Wood Sci 54:45–53. https://doi.org/10.1007/s10086-007-0909-5
28. Ogawa K, Harada M, Shibusawa T, Miyamoto K (2019) Method for measuring the resistances produced on parallel and perpendicular veneers in plywood under nail embedment loading. Dig J Wood Sci. https://doi.org/10.1186/s10086-019-1786-4
29. Obayashi Gumi Public channel (2022) OY Project. https://youtu.be/D4gEmJyEq1c?list=TLGGfPkibFP7jvQxMTA0MjAyMg. Accessed 12 Apr 2022
30. Miyamoto TB, Sinha A, Morrell I (2020) Connection performance of mass plywood panels. For Prod J 70(1):88–99. https://doi.org/10.13073/FPJ-D-19-00056
31. Höglmeier K, Weber-Blaschke G, Richter K (2017) Potentials for cascading of recovered wood from building deconstruction—a case study for south-east Germany. Resour Conserv Recycl 117:304–314. https://doi.org/10.1016/j.resconrec.2015.10.030
32. Japanese Industrial Standards (2009) JIS A 5508 Nails. Japanese Standards Association, Tokyo

33. Leijten AJM (2016) The bearing strength capacity perpendicular to grain of Norway spruce—evaluation of three structural timber design models. Const and Build Mater 105:528–535. https://doi.org/10.1016/j.conbuildmat.2015.12.170

34. Tanahashi H, Shimizu H, Suzuki Y (2006) Elastic surface displacements of orthotropic wood due to partial compression based on Pasternak model. J Struct Eng (AIJ) 609:129–136. https://doi.org/10.3130/aijs.71.129_3

35. Ochiai Y, Aoki K, Inayama M (2018) Fundamental research of an evaluation method of splitting failure in timber ii -effect of specimen shape on splitting strength when loaded parallel to grain. Mokuzaigakkaishi 64(3):94–104. https://doi.org/10.2488/jwrs.64.94

Publisher's Note

Springer Nature remains neutral with regard to jurisdictional claims in published maps and institutional affiliations.